HHS Public Access

Author manuscript

J Appl Toxicol. Author manuscript; available in PMC 2018 November 01.

Published in final edited form as:

J Appl Toxicol. 2017 November ; 37(11): 1297–1304. doi:10.1002/jat.3467.

In vivo Noninvasive Analysis of Graphene Nanomaterials Pharmacokinetics in Mice Using Photoacoustic Detection

Dmitry A. Nedosekin[1,*], **Jacqueline Nolan**[1], **Chengzhong Cai**[1,2], **Shawn E. Bourdo**[3], **Zeid Nima**[3], **Alexandru S. Biris**[3], and **Vladimir P. Zharov**[1]

[1]Arkansas Nanomedicine Center, University of Arkansas for Medical Sciences, Little Rock, AR 722052

[2]National Toxicology Research Center, U.S. Foods and Drug Administration, Jefferson, AR 72132

[3]Center for Integrative Nanotechnology Sciences, University of Arkansas at Little Rock, Little Rock, Arkansas 72204

Abstract

Graphene-based nanomaterials (GBNs) are quickly revolutionizing modern electronics, energy generation and storage, clothing and biomedical devices. Due to a variety of physical and chemical parameters of GBNs that define its toxicity and aggregation of GBNs in suspension, the interpretation of toxicology analysis is challenging without accurate information on graphene distribution and behavior in a live organism. In this work, we present a laser-based optical detection methodology for noninvasive detection of GBNs and its pharmacokinetics analysis directly in blood flow in mice using in vivo photoacoustic (PA) flow cytometry (PAFC). PAFC provides unique insight on how chemical modifications of GBNs affect its distribution in blood circulation and how quickly it is eliminated from the flow. Overall, PA spectroscopy provided a unique data crucial for understanding GBNs toxicity through real-time detection of GBNs using the intrinsic light absorption contrast of these nanomaterials.

Keywords

Photoacoustic; flow cytometry; toxicity; graphene; blood circulation

INTRODUCTION

Graphene based nanomaterials (GBNs) have a tremendous potential in various applications ranging from industry, to energy storage, to consumer electronics and medical applications (Castro Neto, et al. 2009, Mao, et al. 2013, Stankovich, et al. 2006). A widespread use of GBNs would require a detailed understanding of how these materials may interact with live systems at a single cell, as well as at a whole organism levels (Mao, et al. 2013). GBNs consist of mostly carbon atoms arranged in 2D layered sheets (Novoselov, et al. 2004). A toxicity profile of graphene is defined by the number and nature of various groups decorating particles, size and shape of the flakes, surface charge and etc (Duch, et al. 2011,

*Corresponding author: DNedosekin@uams.edu, Phone: +1 (501) 526 7620.

Mao, et al. 2013). Complex chemistry of GBNs would also dictate its pharmacokinetic profile and possible toxic effects on live systems upon exposure (Mao, et al. 2013, Sanchez, et al. 2012, Yang, et al. 2011).

One of the major complications in the research of GBNs is the fact that identification of carbon-based nanomaterials in carbon-rich biological samples is very hard using conventional analytical techniques. Programmed thermal analysis (Doudrick, et al. 2015), requiring sample destruction, was proposed for wastewater biomass analysis. Raman spectroscopy has been proposed for spectral identification and mapping of carbon nanomaterials in cells (Majeed, et al. 2016) in vitro. In vivo GBNS were analyzed using GBNs radio-labeled with 14C (Mao, et al. 2015) or 125I (Badun, et al. 2016, Yang, et al. 2011), as well as particles decorated with fluorescent tags (Yang, et al. 2010)(Wang, 2016). In most cases radio-labeling and graphene decorating with tags either requires synthesis of completely new material and cannot be applied toward existing products, or decoration may change the chemistry of GBNs since chemical modification is needed to attach tags to the particle surface.

Most of GBNs have unique optical properties and exceptionally high light absorption contrast (Bonaccorso, et al. 2010, Koppens, et al. 2011) with each single layer of graphene absorption as much as 2.3 % of incident light in a wide range of wavelengths. This opens up a possibility toward detection of GBNs using their intrinsic light absorption through the use of photoacoustic (PA) detection techniques. PA spectroscopy is utilizing light absorption contrast for quantification of proteins, dyes and nanoparticles (Cox, et al. 2012, Hu 2016, Liu and Zhang 2016, Wang, et al. 2016, Wu, et al. 2014). High contrast of GBNs prompted development of graphene-based contrast agent for PA imaging (Mao, et al. 2013, Moon, et al. 2015, Patel, et al. 2013, Sheng, et al. 2013). The advantages of PA detection of GBNs include non-destructiveness and analysis of light scattering tissues including deep vessels.

Herewith, we present PA based flow cytometry technique for noninvasive detection and monitoring of circulating GBN particles *in vivo* in whole mouse blood. For mice this non-invasive approach requiring no blood sampling provides a possiblity to dramatically reduce the number of animals and overall research cost. We demonstrate that PA flow cytometry (PAFC) has detection sensitivity sufficient for detection of single GBN flakes *in vivo* and provides real-time information on concentration of GBNs in flow revealing differences in pharmacokinetics of circulating GBNs with hydrophobic and hydrophilic surfaces.

MATERIALS AND METHODS

Graphene based nanomaterials

Three types of GBNs were analyzed in this work: few layer poweder of pristine graphene (N002-PDR, lot# DR5014043001, purchased from Angstron Materials, Dayton, OH), functionalized graphene (f-graphene) made from N002-PDR graphene powder by treating it with 600 mL of H_2SO_4 (Certified ACS Plus, Fisher Chemical, 95.0 to 98.0 w/w % F.W. 98.08) and 200 mL of concentrated HNO_3 (Certified ACS Plus 70%, Fisher Chemical, F.W. 63.01), and graphene oxide (N002-PS, lot# S2071112, Angstron Materials, Dayton, OH). As purchased pristine graphene had flakes of various diameter and thickness of 1–1.2 nm and

was highly hydrophobic. It formed clusters up to 10 μm in diameter persistent even after aggressive sonication (Supplementary Figure S1). Upon chemical treatment (Majeed, et al.) functionalized graphene was decorated with some hydrophilic alcohol and carboxylic acid groups, that rendered less hydrophobic and had fewer large clusters. X-ray photoelectron spectroscopy analysis (Bourdo, et al. 2017, Majeed, et al.) demonstrated a ~ 6.63±0.14% oxygen content increase compared to ~2.5% for initial graphene powder. Graphene oxide (≤ 46% of oxygen, manufacturer data, Supplementary Information Table S1) was finely dispersed in water and fromed a stable suspension in water without any significant precipitation observed over more than 2 years of shelf storage. All GBN solutions for injection were prepared in 1X phosphate buffered saline (PBS, Gibco, Life Technologies) with a final concentration of GBNs in the range 25 – 250 μg/mL.

Animal model

All the animal protocols were approved by the University of Arkansas for Medical Sciences Institutional Animal Care and Use Committee. *In vivo* PA detection was performed in mouse ears in 35–45 μm sized blood vessels of nude (nu/nu) mice (female, 8–10 weeks old, weighing 20–30 g, procured from Charles River Breeding Laboratories, Wilmington, MA). Mice were kept in normal environment (RH = 55%–65%, T = 20–24 C, normal light cycles) at UAMS DLAM facility. For PA monitoring animals were anesthetized using Isoflurane (inhalation, 1.2%), and placed on a temperature-controlled stage (37°C) of the custom microscope. 50 μL solution of GBNs (at concentrations ranging from 25 to 250 μg/mL) was introduced using either mouse tail vein injection. The typical duration of PA experiment was ~ 60 min including at least 40 min long monitoring of PA signals after injection. Mice were euthanized using CO_2 chamber after PA monitoring, while still under Isoflurane anesthesia.

In vitro calibration of PA detection of GBNs was performed using whole blood from control nu/nu mice (not injected with GBNs). Terminal whole blood samples (cardiac puncture, up to 1 mL sample volume) were collected using plastic syringes and stabilized with K2EDTA (10 μL of 10% solution per 1 mL of blood). Blood samples were kept on ice, spiked with GBNs solution and gently mixed by several tube inversions. For PA analysis the inlet end of the quartz capillary was inserted directly into the test with whole blood sample.

Laser scanning PA microscopy

The custom laser scanning PA microscope was based on Olympus IX81 inverted microscope platform. Laser scanner was based on XY galvo mirrors (GVSM002, Throlabs Inc., Newton, NJ), pulsed lasers were coupled to the microscope via single mode optical fibers. The system was equipped with nanosecond lasers: 532 nm (LUCE 532, Bright Solutions, Italy), 671 nm (CrystaLaser, Reno NV) and 1064 nm (MOPA-M-10, MultiWave Photonics, Portugal) focused into the sample by a 10× objective (DPlan 10×, Olympus Inc). Acoustic waves were acquired by a non-focused 4.5 MHz transducer (model 6528101, 3.5 MHz, 4.5 mm in diameter; Imasonic Inc., Besançon, France) placed over the sample (transmission configuration). Signals from the transducer were amplified by a 20 dB amplifier (0.05–100 MHz bandwidth, AH-2010–100, Onda Corp.) and recorded by a PC equipped with a high-speed digitizer (PCI-5124, 12-bit card, 128 MB of memory, National Instruments, Austin, TX). System synchronization and laser triggering were performed by a digital waveform

generator (DG4062, Rigol, Beijun, China). Laser beam spot size was estimated to be ~ 0.9 μm (FWHM) and laser step scan was 1 μm. For each sample point maximal amplitude of the acoustic wave was recorded. Optical microscopy images were collected by DP72 camera (Olympux Inc) using a custom ring illuminator mounted on the transducer, Figure 1B.

In vivo Photoacoustic Flow Cytometer

PAFC setup has been described in detail elsewhere (Nedosekin, et al. 2013),(Nedosekin, et al. 2014). Here, PAFC setup was equipped with 10 kHz 671 and 820 nm high pulse repetition rate lasers (CrystLaser, Reno, NV and Luce 820 Bright Solutions, Italy, respectively) for PA detection. Laser beams were focused into a square shaped quartz capillary having 100μm internal diameter (*in vitro* PAFC) or into a mouse ear blood vessel (*in vivo* PAFC) PA signals from the circulating objects were acquired by an unfocused ultrasound transducer (model 6528101, 3.5 MHz, 5.5 mm in diameter; Imasonic Inc., Besancon, France). Signals from transducer were amplified (amplifier model 5662B, 50kHz – 4 MHz; Panametrics) and recorded by PC.

In vitro analysis of blood samples

200 μL blood aliquots were spiked with 5 μL of GBNs solution in PBS to achieve a final concentration of GBNs in the range 50 ng/mL to 25 μg/mL. Blood samples were pulled through a square quartz capillary (100 μm i.d., Polymicro Tech., Molex, Phoenix AZ) by a syringe pump (KDS 200, withdraw mode, KD Scientific, Holliston, MA) at a rate of 1 mL/h, Figure 2C. PA signals were recorded for ~ 2 min for each sample (16 μL tested sample volume). Transient PA signals exceeding detection threshold set up for control blood were counted within 10 s long intervals for each sample (~2 μL blood volume per interval) and used to calculate the calibration graph. A tiny sample of GBN spiked blood was diluted with PBS and placed into a 35 mm round dish for PA microscopy analysis.

In vivo PA visualization of circulating GBNs clusters in blood vessels

In vivo PA visualization of GBNs in live mouse tissues has been performed by high speed PA laser scanning microscope visualizing tissues and blood vessels through a window chamber implanted in mouse skin fold (Bao, et al. 2013). Mice were anesthetized using 1.2 % Isoflurane, placed on a heated stage with glass side of the window chamber facing focusing objective. Skin on the other side of the window chamber was covered with ultrasound gel for acoustic matching. Ultrasound transducer was carefully positioned over the analyzed area. PA images were collected either at a speed of 8 Hz (50×50 pixels) or 0.25 Hz (200×200 pixels). Laser energy was 10 μJ/pulse and no tissue damage was observed after PA imaging. 50 μL of functionalized graphene at 125 μg/mL was injected through tail vein.

In vivo PA flow cytometry analysis of GBNs pharmacokinetics

In vivo PA analysis of GBNs in mouse blood was performed on 40μm ear arteries using PAFC system. Anesthetized mouse (1.2% Isoflurane) was placed on a heated stage with ear spread flat on a glass coverslip. Transducer was placed over the ear with ultrasound gel used for acoustic coupling. 50 μL of GBNs solution at concentration of 125 μg/mL was injected through a tail vein and PA signals from the artery were recorded for 40–60 min after that.

For each GBN we performed 5–7 injections (each time a new mouse was used) with a goal of achieving at least satisfactory 5 PA recordings per group.

Statistical Analysis

PAFC data trace analysis and statistical calculations were performed using custom LabView (national Instruments, Austin, TX) software, which identified transient PA signals exceeding a certain threshold. The threshold was calculated using local mean PA signal (to account for baseline fluctuations) and “no-even” PA signal value calculated from the control data traces (before injection or control blood with no GBNs) for each experiment. This ensured absence of false-positive signals in the recording. Next, identified PA peaks were either counted directly or all the PA signals over a certain threshold were integrated (10 to 40 s time bin) to account for differences in PA signal amplitudes from single flakes and large clusters. PA data was presented as raw traces, integrated PA signal or, when appropriate, as mean PA signal ± standard deviation.

RESULTS

PA contrast of GBNs in blood

PA contrast of GBNs is determined by the non-radiative relaxation of absorbed light into heat. Each carbon layer of GBNs absorbs incident light (Bonaccorso, et al.), thus even a few-layers-thick flake have a significant PA contrast. PA microscopy confirmed that functionalized graphene can be identified among red blood cells (RBCs), Figure 1A, using only intrinsic light absorption of GBNs in the tissue transparency window. PA signal at 532 nm was mostly dominated by hemoglobin, while at 671 nm graphene had high contrast and hemoglobin signal was negligible. Spectroscopy of hemoglobin and graphene solutions, Figure 1C, indicate good contrast of graphene both in the tissue transparency window (630 to 900 nm), and at clinically relevant 1064 nm wavelength, where low cost of high energy pulsed lasers and low tissue scattering provide an optimal combination (Nedosekin, et al. 2010). In microscopy mode we estimated the sensitivity of PA measurements by acquiring signals from graphene clusters of different sizes, Figures 1D and 1E. A large laser spot (20 μm) was selected to ensure that the whole cluster is illuminated. Overall, detection sensitivity was estimated to correspond to a single few layer thick flake with a diameter of ~ 250 nm; however, accurate cluster/flake size measurements of such size were not possible in the selected microscope configuration, thus more accurate sensitivity estimation may require controlled graphene deposition to build a calibration standard material.

PA counting of GBNs flakes in whole blood under flow conditions

In order to prove the concept that PA detection in flow is sufficient for accurate enumeration of circulating GBN flakes we designed an *in vitro* phantom featuring a 100 μm i.d. quartz capillary tube immersed in acoustic gel. Blood samples were spiked with *f*-graphene and PA signal trace from spiked samples demonstrated the presence of multiple transient high-amplitude PA signals that were not observed in control blood samples. Figure 2 shows typical examples of PA traces with f-graphene peaks having amplitudes up to 2 orders of magnitude higher than blood background. The distribution of PA peak amplitudes was very wide reflecting the fact that f-graphene tends to form clusters and aggregates. However, the

calibration based on the number of observed peaks was linear and sufficient for prediction of GBNs concentration in the sample. The sensitivity of detection was proportional to the duration of data acquisition and total sample volume. The system used in this project was capable of pulling 1 mL of whole blood in ~ 1h allowing for a potential increase in sensitivity by extending 1 s long data sections up to 1h long intervals, i.e. up to 3600 times. We also observed some clustering of the graphene with white blood clots (formed by white blood cells) that had a dual “positive-negative” PA contrast (Supplementary Figure S2), since white clots included little or none RBCs and provided a decreased PA background (no hemoglobin).

Optimization of noninvasive PA analysis of GBNs pharmacokinetics in mouse blood circulation

The injection of 50 μL of f-graphene solution at concentrations of 250 μg/mL, 125 μg/mL and 25 μg/mL (a total of 12.5, 6.25 and 1.25 μg of the graphene, respectively) was used to optimize the concentration and total amount of GBNs required for the PA analysis of circulating GBNs, Figure 3A. The injection of concentrated (250 μg/mL) f-graphene solution caused significant changes in mouse breathing and led to the death of several mice (possibly, due to clogging of pulmonary vessels). Interestingly, slightly more diluted solution (125 μg/mL) was tolerated better and caused fewer side effects in relation to blood flow, and no mice were lost. Overall, the PA traces recorded for all the concentrations tested correlated very well and revealed a quick decrease in the number of observed PA peaks across all the samples. This preliminary data highlighted that PA sensitivity is sufficient for detection of individual flakes and clusters in flow and provides temporal resolution unattainable by invasive methods. In order to assess the changes in the number of observed PA signals over time we either calculated the number of PA signals per a certain period of time, Figure 3C, or summed up the amplitudes of all the PA signals exceeding a certain threshold. The latter case better allows accounting for differences in mass of clusters (high PA signals) and single flakes (low amplitude PA signals). Calculation of the average PA signal from GBNs over a certain time frame allowed minimization of the random distribution of GBNs in flow. Still, some physiological factors remained including sudden changes in blood flow that decreased an observed concentration of GBNs, Figure 3C (125 μg/mL data for the time period 17 to 22 min after the injection). For all the further experiments we selected the injection of 125 μg/mL solution that produces sufficient number of PA peaks for accurate statistical analysis of GBNs in circulation, while it had minimal effect on the animal during the procedure.

Reproducibility of *in vivo* PA analysis

A single PA trace provides detailed real-time data on the presence of GBNs in blood. However, a comparison of PA traces between animals may be complicated due to differences in the amount of injected materials, differences in ear blood vessel size and flow rate and overall mouse conditions, including transient changes caused by the injection of potentially toxic compounds. For example, after the injection of GBNs we often observed temporal decline in blood flow velocity and/or blood vessel contraction/dilation. In order to assess how reproducible the results of PA analysis of GBNs pharmacokinetics are, we analyzed PA traces for 5 animals injected with identical amount of functionalized graphene solution, Figure 4A. Overall, the number of peaks and integrated PA signals varied dramatically with

up to 10-folds difference in the amount of the material detected right after injection. However, the long term monitoring, Figure 4B, shows that general trends are similar, especially in the short term, when the majority of the nanomaterial is removed from circulation and/or redistributed throughout the whole blood volume. The analysis of PA data, Figure 4B, shows that two distinct regions can be identified. First, a fast exponential decline in GBNs concentration takes place for approximately 10 min after injection. This region is well reproduced in all the mice. It is followed, by a second slower process, when the concentration of particles is still decreasing, but not as fast. Lower reproducibility of the second curve is most probably related to the fact that lower number of peaks are detected, leading to a decreased significance of the measured GBNs concentration using PA data traces.

Pharmacokinetics of hydrophobic and hydrophilic GBNs

The PA flow cytometry can reveal differences in how GBNs that have different chemical properties are distributed in blood during circulation. We analyzed PA data traces after injection of pristine graphene (hydrophobic), functionalized graphene (partially hydrophilic) and graphene oxide (hydrophilic flakes). The difference in hydrophobicity affected stability of the flakes in water suspensions. The most stable solution without any visible aggregates was formed by graphene oxide. Both commercial and functionalized graphene samples quickly precipitated and only a minor fraction of the material remained in the solution. PA detection has confirmed these GBNs behave differently in blood circulation. Graphene oxide had very uniform distribution of signal amplitudes. There were no PA signatures observed that we usually correlate with large GBN clusters (high amplitude, wide peaks in PA trace), Figure 5A. For both pristine and functionalized graphene samples, Figures 5B and 5C, PA traces reveal high heterogeneity of PA signal amplitudes that indicates the presence of clusters. Moreover, in pristine graphene there were very few low amplitude peaks that usually correspond to single, individual flakes of GBNs.

Surprisingly, the analysis of integrated PA signal shows that the general trends of a decline in the number and intensity of PA signals are very close for both very hydrophilic graphene oxide and only partially hydrophilic functionalized graphene. This correlates with the fact that identical amounts were injected into circulation. However, we assumed that due to different surface chemistry the elimination dynamic would be dramatically different. In the case of pristine graphene, the dynamic curve does not allow making a conclusion regarding changes in the concentration due to the presence of rare large clusters randomly entering the detection zone.

DISCUSSION

PA detection provides a unique approach toward noninvasive detection of GBNs directly in blood flow and a trove of unique data to correlate toxicity manifestations with the pharmacokinetic profile for the nanomaterial. To the best of our knowledge this is the only technique that allows for noninvasive monitoring of single GBN flakes in whole blood circulation. Moreover, most of the conventional analytical techniques are not suitable for identification of single carbon-based flakes of the nanomaterial in carbon-rich samples

(blood or tissues) even *ex vivo*. The PA contrast of GBNs is based on intrinsic light absorption of the nanomaterial and, thus, does not require any chemical modification (labeling of the flakes with fluorescent or radioactive tags). Chemical modifications of GBNs to attach such tags may dramatically change properties of the nanomaterial including its potential toxicity. Here, both pristine graphene (most likely to be used in industry applications) and graphene oxide (high potential for biomedical application) were analyzed as is, without any chemical modifications.

The major advantage of *in vivo* monitoring is that it provides real-time data on concentration of GBNs, which is not feasible if blood has to be sampled to quantify GBNs. This dramatically reduces the number of animals required to study the pharmacokinetics of nanomaterials and the cost of research. Another advantage of PA flow cytometry demonstrated here is that PA data traces directly show whether the nanomaterial is aggregated or homogeneously distributed. The overall amount of graphene, as demonstrated by the integrated PA signal data, Figure 5, was close for the analyzed GBNs; however PA traces show that there is a dramatic difference in the behavior of the NPs in flow (clusters vs single flakes). Here, we hypothesize that similar dynamics of GBNs in circulation could be related to a rapid coating of the hydrophobic nanomaterials with blood serum proteins; however, more experiments would be required to prove this.

Certainly, the technique presented here has disadvantages. First, the rate of graphene signals dramatically depends on blood flow velocity in the vessel and vessel size. Here, we assumed that volume blood flow rate is identical for all the mice analyzed. This assumption can be easily corrected by real-time tracking of the flow rate, and it is possible to alter the current PA experiment design to extract such data directly from PA data traces (Nolan, et al. 2016, van den Berg, et al. 2015). Second, the amount of injected nanomaterial and the loss of the material during injection increase data variability. Figure 4 shows that an absolute count of GBN peaks may differ greatly for different mice/injections, however it is also true for other techniques relying on i.v. injection. A possible solution to this problem may include a co-injection of a standard solution of fluorescent beads to be detected independently (Supplementary Figure S3) using fluorescence modality of an *in vivo* flow cytometer (Nedosekin, et al. 2013). Third, the PA signal from large aggregates can be nonlinearly enhanced through formation of gas bubbles around overheated nanoparticles (Sarimollaoglu, et al. 2014). In this case the amount of clustered nanomaterial can have a higher impact on the overall PA signal compared to single flakes. This would require a careful calibration of PA signals from flakes and clusters of different size. At the moment it is not clear how much the effects of nonlinear amplification could affect our data. Overall, the direct correlation of the acquired PA signals with the mass of GBNs in circulation is not possible since there are no standard calibration materials that could be injected in order to calibrate PA signal response. Still, even direct counting of peaks (Fig 2B) or integrated PA signals (Fig. 5) may provide sufficient data on relative changes in GBNs concentration and/or clustering status. Finally, the PAFC system is not able to distinguish between co-injected GBNs with different chemistry or between GBN and other carbon-based nanomaterials since their absorption spectra are almost identical. This is rather insignificant in pharmacokinetic studies, but may complicate application of the technique in analysis of environmental exposure, or if a mixture of different nanoparticles is proposed as a drug carrier.

The PA system used in this work was optimized for detection of pigmented cells and nanoparticles in mouse ear veins; however, for other animals thicker skin can dramatically reduce detection sensitivity. This effect can be minimized either through the use of a different PA cytometer optimized for thick samples though the use of acoustic focusing (Menyaev, et al. 2013) or by removing skin and installing a glass window chamber to have an ultimate access to blood vessels under skin. While an invasive procedure (Shao, et al. 2013), the window chamber would allow transferring our technology to any animal model and even increase detection sensitivity. In this work, we focused only on detection and enumeration of GBN flakes in blood and analysis of pharmacokinetics for different GBNs materials. However, PA detection can be easily extended to analysis of other biological fluids and tissues including whole animal imaging using PA tomography (Bao, et al. 2013) and label free mapping of graphene in histological tissue sections (Cook, et al. 2013, Nedosekin, et al. 2010).

CONCLUSIONS

We have presented here a novel technique for noninvasive detection and analysis of pharmacokinetic profile for potentially toxic carbon-based nanomaterials in blood circulation. PA detection allowed real-time label-free monitoring of different GBNs in whole blood with sensitivity reaching levels corresponding to single flakes of graphene in the detection volume. The analysis of GBNs having different surface chemistry has demonstrated that while overall dynamics of GBNs clearance from circulation was relatively similar. The hydrophilic material (graphene oxide) was circulating mostly as single flakes, while pristine graphene (hydrophobic material) and functionalized graphene (partially hydrophobic material) formed multiple large clusters in circulation.

Supplementary Material

Refer to Web version on PubMed Central for supplementary material.

Acknowledgments

The authors declare that there are no conflicts of interest. This work was supported by grants from the National Institutes of Health (R01CA131164, R01EB009230, R01EB017217, R21EB0005123, and R21CA139373), the National Science Foundation (DBI-0852737). This work was also supported by the U.S. Food and Drug Administration (award HHSF223201210189C administered through Arkansas Research Alliance). The views presented in this paper are not necessarily those of the U.S. FDA. Partial funding for this project was provided by the Center for Advanced Surface Engineering, under the National Science Foundation Grant No. IIA-1457888 and the Arkansas EPSCoR Program, ASSET III.

References

Badun GA, Chernysheva MG, Grigorieva AV, Eremina EA, Egorov AV. Langmuir hydrogen dissociation approach in radiolabeling carbon nanotubes and graphene oxide. Radiochimica Acta. 2016:593.

Bao C, Beziere N, del Pino P, Pelaz B, Estrada G, Tian F, Ntziachristos V, de la Fuente JM, Cui D. Gold nanoprisms as optoacoustic signal nanoamplifiers for in vivo bioimaging of gastrointestinal cancers. Small. 2013; 9:68–74. DOI: 10.1002/smll.201201779 [PubMed: 23001862]

Bonaccorso F, Sun Z, Hasan T, Ferrari AC. Graphene photonics and optoelectronics. Nat Photon. 2010; 4:611–622. DOI: 10.1038/Nphoton.2010.186

Bourdo S, Al Faouri R, Sleezer R, Nima Z, Lafont A, Chhetri B, Benamara M, Martin B, Salamo G, Biris A. Physicochemical characteristics of pristine and functionalized graphene. J Appl Toxicol. 2017 under review.

Castro Neto AH, Guinea F, Peres NMR, Novoselov KS, Geim AK. The electronic properties of graphene. Rev Mod Phys. 2009; 81:109–162.

Cook JR, Frey W, Emelianov S. Quantitative Photoacoustic Imaging of Nanoparticles in Cells and Tissues. ACS nano. 2013; 7:1272–1280. DOI: 10.1021/nn304739s [PubMed: 23312348]

Cox B, Laufer JG, Arridge SR, Beard PC. Quantitative spectroscopic photoacoustic imaging: a review. J Biomed Opt. 2012; 17:061202.doi: 10.1117/1.jbo.17.6.061202 [PubMed: 22734732]

Doudrick K, Nosaka T, Herckes P, Westerhoff P. Quantification of graphene and graphene oxide in complex organic matrices. Environ Sci Nano. 2015; 2:60–67. DOI: 10.1039/C4EN00134F

Duch MC, Budinger GR, Liang YT, Soberanes S, Urich D, Chiarella SE, Campochiaro LA, Gonzalez A, Chandel NS, Hersam MC, Mutlu GM. Minimizing oxidation and stable nanoscale dispersion improves the biocompatibility of graphene in the lung. Nano Lett. 2011; 11:5201–5207. DOI: 10.1021/nl202515a [PubMed: 22023654]

Hu S. Emerging concepts in functional and molecular photoacoustic imaging. Curr Opin Chem Biol. 2016; 33:25–31. DOI: 10.1016/j.cbpa.2016.04.003 [PubMed: 27111279]

Koppens FHL, Chang DE, de Abajo FJG. Graphene Plasmonics: A Platform for Strong Light-Matter Interactions. Nano Letters. 2011; 11:3370–3377. DOI: 10.1021/Nl201771h [PubMed: 21766812]

Liu W, Zhang HF. Photoacoustic imaging of the eye: A mini review. Photoacoustics. 2016; 4:112–123. DOI: 10.1016/j.pacs.2016.05.001 [PubMed: 27761410]

Majeed W, Bourdo S, Petibone DM, Saini V, Vang KB, Nima ZA, Alghazali KM, Darrigues E, Ghosh A, Watanabe F, Casciano D, Ali SF, Biris AS. The role of surface chemistry in the cytotoxicity profile of graphene. J Appl Toxicol. 2016; n/a-n/a. doi: 10.1002/jat.3379

Mao HY, Laurent S, Chen W, Akhavan O, Imani M, Ashkarran AA, Mahmoudi M. Graphene: promises, facts, opportunities, and challenges in nanomedicine. Chem Rev. 2013; 113:3407–3424. DOI: 10.1021/cr300335p [PubMed: 23452512]

Mao L, Hu M, Pan B, Xie Y, Petersen EJ. Biodistribution and toxicity of radio-labeled few layer graphene in mice after intratracheal instillation. Part Fibre Toxicol. 2015; 13:7.doi: 10.1186/s12989-016-0120-1

Menyaev YA, Nedosekin DA, Sarimollaoglu M, Juratli MA, Galanzha EI, Tuchin VV, Zharov VP. Optical clearing in photoacoustic flow cytometry. Biomed Opt Express. 2013; 4:3030–3041. DOI: 10.1364/boe.4.003030 [PubMed: 24409398]

Moon H, Kumar D, Kim H, Sim C, Chang JH, Kim JM, Kim H, Lim DK. Amplified photoacoustic performance and enhanced photothermal stability of reduced graphene oxide coated gold nanorods for sensitive photoacoustic imaging. ACS Nano. 2015; 9:2711–2719. DOI: 10.1021/nn506516p [PubMed: 25751167]

Nedosekin DA, Sarimollaoglu M, Galanzha EI, Sawant R, Torchilin VP, Verkhusha VV, Ma J, Frank MH, Biris AS, Zharov VP. Synergy of photoacoustic and fluorescence flow cytometry of circulating cells with negative and positive contrasts. J Biophotonics. 2013; 6:425–434. DOI: 10.1002/jbio.201200047 [PubMed: 22903924]

Nedosekin DA, Sarimollaoglu M, Shashkov EV, Galanzha EI, Zharov VP. Ultra-fast photoacoustic flow cytometry with a 0.5 MHz pulse repetition rate nanosecond laser. Opt Express. 2010; 18:8605–8620. DOI: 10.1364/oe.18.008605 [PubMed: 20588705]

Nedosekin DA, Shashkov EV, Galanzha EI, Hennings L, Zharov VP. Photothermal Multispectral Image Cytometry for Quantitative Histology of Nanoparticles and Micrometastasis in Intact, Stained and Laser Burned Tissues. Cytometry. 2010; 77:1049–1058. DOI: 10.1002/cyto.a.20977 [PubMed: 20949577]

Nedosekin DA, Verkhusha VV, Melerzanov AV, Zharov VP, Galanzha EI. In vivo photoswitchable flow cytometry for direct tracking of single circulating tumor cells. Chem Biol. 2014; 21:792–801. DOI: 10.1016/j.chembiol.2014.03.012 [PubMed: 24816228]

Nolan J, Sarimollaoglu M, Nedosekin DA, Jamshidi-Parsian A, Galanzha EI, Kore RA, Griffin RJ, Zharov VP. In Vivo Flow Cytometry of Circulating Tumor-Associated Exosomes. Anal Cell Pathol (Amst). 2016; 2016:1628057.doi: 10.1155/2016/1628057 [PubMed: 27965916]

Novoselov KS, Geim AK, Morozov SV, Jiang D, Zhang Y, Dubonos SV, Grigorieva IV, Firsov AA. Electric Field Effect in Atomically Thin Carbon Films. Science. 2004; 306:666–669. DOI: 10.1126/science.1102896 [PubMed: 15499015]

Patel MA, Yang H, Chiu PL, Mastrogiovanni DD, Flach CR, Savaram K, Gomez L, Hemnarine A, Mendelsohn R, Garfunkel E, Jiang H, He H. Direct production of graphene nanosheets for near infrared photoacoustic imaging. ACS Nano. 2013; 7:8147–8157. DOI: 10.1021/nn403429v [PubMed: 24001023]

Sanchez VC, Jachak A, Hurt RH, Kane AB. Biological Interactions of Graphene-Family Nanomaterials: An Interdisciplinary Review. Chem Res Toxicol. 2012; 25:15–34. DOI: 10.1021/Tx200339h [PubMed: 21954945]

Sarimollaoglu M, Nedosekin DA, Menyaev YA, Juratli MA, Zharov VP. Nonlinear photoacoustic signal amplification from single targets in absorption background. Photoacoustics. 2014; 2:1–11. DOI: 10.1016/j.pacs.2013.11.002 [PubMed: 24921062]

Shao J, Griffin RJ, Galanzha EI, Kim JW, Koonce N, Webber J, Mustafa T, Biris AS, Nedosekin DA, Zharov VP. Photothermal nanodrugs: potential of TNF-gold nanospheres for cancer theranostics. Sci Rep. 2013; 3:1293.doi: 10.1038/srep01293 [PubMed: 23443065]

Sheng Z, Song L, Zheng J, Hu D, He M, Zheng M, Gao G, Gong P, Zhang P, Ma Y, Cai L. Protein-assisted fabrication of nano-reduced graphene oxide for combined in vivo photoacoustic imaging and photothermal therapy. Biomaterials. 2013; 34:5236–5243. DOI: 10.1016/j.biomaterials.2013.03.090 [PubMed: 23602365]

Stankovich S, Dikin DA, Dommett GH, Kohlhaas KM, Zimney EJ, Stach EA, Piner RD, Nguyen ST, Ruoff RS. Graphene-based composite materials. Nature. 2006; 442:282–286. DOI: 10.1038/nature04969 [PubMed: 16855586]

van den Berg PJ, Daoudi K, Steenbergen W. Review of photoacoustic flow imaging: its current state and its promises. Photoacoustics. 2015; 3:89–99. DOI: 10.1016/j.pacs.2015.08.001 [PubMed: 26640771]

Wang D, Wu Y, Xia J. Review on photoacoustic imaging of the brain using nanoprobes. Neurophoton. 2016; 3:010901.doi: 10.1117/1.NPh.3.1.010901

Wu D, Huang L, Jiang MS, Jiang H. Contrast agents for photoacoustic and thermoacoustic imaging: a review. Int J Mol Sci. 2014; 15:23616–23639. DOI: 10.3390/ijms151223616 [PubMed: 25530615]

Yang K, Wan J, Zhang S, Zhang Y, Lee ST, Liu Z. In vivo pharmacokinetics, long-term biodistribution, and toxicology of PEGylated graphene in mice. ACS Nano. 2011; 5:516–522. DOI: 10.1021/nn1024303 [PubMed: 21162527]

Yang K, Zhang S, Zhang G, Sun X, Lee ST, Liu Z. Graphene in mice: ultrahigh in vivo tumor uptake and efficient photothermal therapy. Nano Lett. 2010; 10:3318–3323. DOI: 10.1021/nl100996u [PubMed: 20684528]

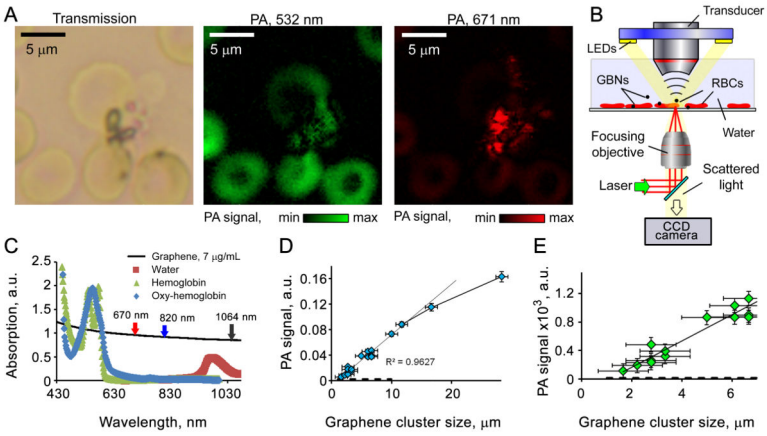

Figure 1.

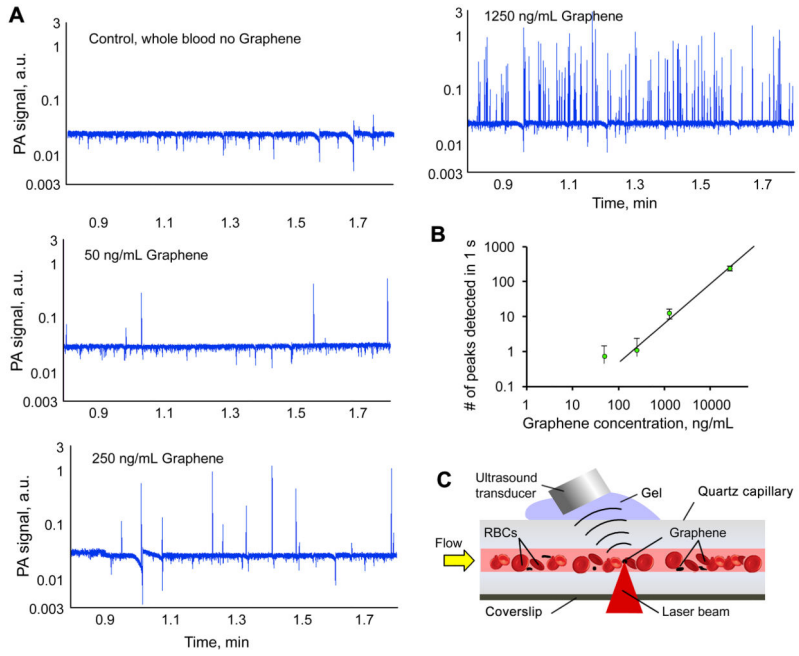

Figure 2.

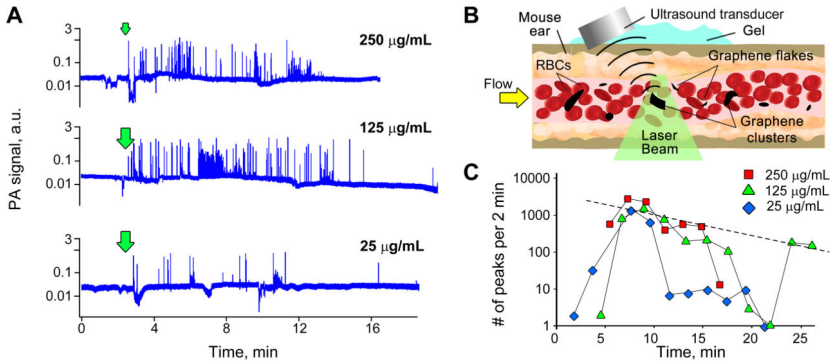

Figure 3.

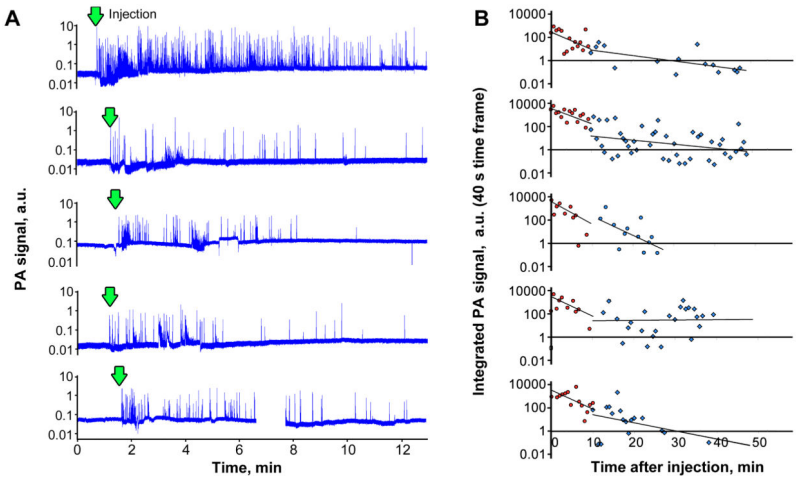

Figure 4.

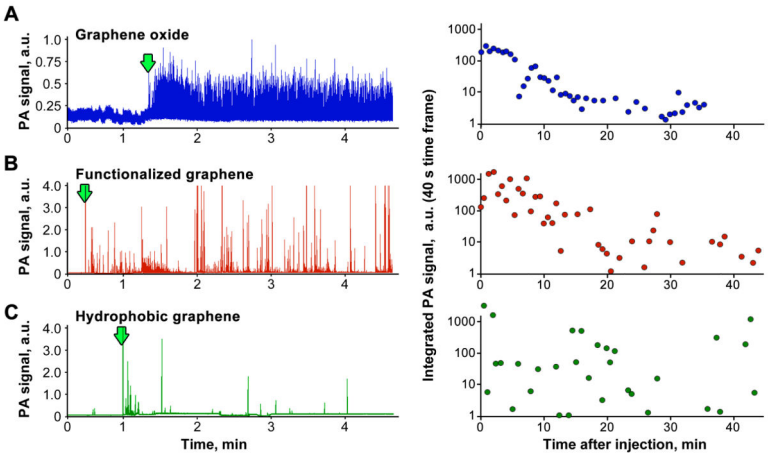

Figure 5.